TASK QUARTERLY 5 No 2 (2001), 165–178

NUMERICAL INVESTIGATION OF THE SECONDARY FLOW DEVELOPMENT IN TURBINE CASCADE

PIOTR DOERFFER[1], JAROSŁAW RACHWALSKI[1]
AND FRANCO MAGAGNATO[2]

[1]*Institute of Fluid Flow Machinery,*
Polish Academy of Sciences,
Fiszera 14, 80-952 Gdansk, Poland
doerffer@imp.gda.pl, viking@imp.gda.pl

[2]*Fachgebiet Strömungsmaschinen, University of Karlsruhe,*
Kaisserstr. 12, D-76 128 Karlsruhe, Germany
magagnato@mach.uni-karlsruhe.de

(Received 23 February 2001)

Abstract: The results represent the first attempt of the numerical analysis of 3-D secondary flows formed in the linear turbine cascade wind tunnel. Numerical simulations were carried out by means of the SPRC code [1]. It was possible to make the calculations presented here thanks to the cluster of PC's providing sufficient computational resources. In order to be able to verify the obtained results the case considered is the workshop test case [2]. It has been shown that the obtained results are in very good agreement with experiment. This gave confidence in the results and several important conclusions concerning the development of streamwise vortices could be made thanks to the work carried out.

Keywords: turbines, Computational Fluid Dynamics, secondary flows

1. Introduction

The research work concerning flow development in turbine cascade is focused nowadays on small details of a flow field such as: laminar – turbulent transition, shock wave – boundary layer interaction, flow separation, formation and behaviour of streamwise vortices as well as coolant bleeding effects on 3-D structure of secondary flows. These flow phenomena are so complex that to study them in detail a simplified geometry such as linear cascade should be used.

Linear cascade flow investigation has a long history especially in experimental investigations. These were mostly compared with 2-D numerical analysis. Nowadays substantial work is directed towards the detection of 3-D effects. Three dimensionality of the flow in linear cascades has been studied by many authors [3–5] and [6] additionally treated some methods of secondary flow control.

One of the tools of analysis under development at O2/Z2 in the IMP PAN is numerical simulation. Code SPARC described in [1] and originating from Karlsruhe is well suited for the purpose of secondary flow analysis because it is a 3-D code for viscous and compressible flows. In order to learn about all important aspects of numerical simulations of 3-D flow through a turbine cascade the case of configuration presented in [2] was considered. This case is well documented experimentally and also several results of numerical simulations are presented in [2]. Therefore sufficient comparison material is available.

The main goal of the presented here paper is to try to obtain all details of the secondary flow structure. If the flow structure is well reproduced it will be possible to trace and analyse the origin and development of streamwise vortices. This work is also a starting point for the analysis of the interaction between the secondary flow and the coolant injection which is planned for the nearest future.

2. Secondary flow formation

In order to clarify the basis for further discussion it is necessary to summarise what is widely discussed in literature concerning the secondary flow structure. In Figure 1 the components of streamwise vortices configuration are indicated.

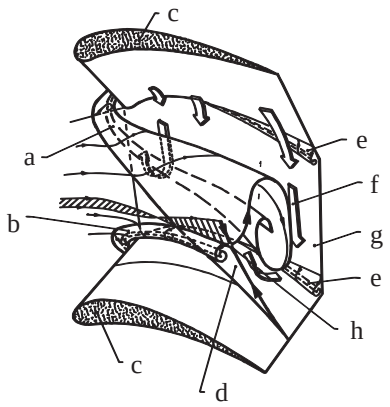

Figure 1. Secondary flow structure: a – horse shoe vortex pressure side; b – horse shoe vortex suction side; c – blade; d – dividing stream surface; e – corner vortex; f – passage vortex; g – side wall; h – saddle point

These usually become the places of concentration of losses because in nature they roll up the low momentum layers. Within blade passage these are:

- horse shoe vortex, generated by the blade leading edge; it rolls up the side wall boundary layer;
- passage vortex, represents the rollup of the cross flow at the side wall between blades;
- corner vortices, which represent separation of the passage vortex in corners;
- separation shear sheet, bordering the undisturbed main stream from the secondary flow.

Due to a different spanwise flow deflection at both sides of the trailing edge a spanwise vorticity is produced within the wake. Downstream the trailing edge this vorticity sheet may roll up into an additional trailing shed vortex. This vortex being formed downstream the

cascade may be significantly affected by vortices generated upstream in the blade passage. The mechanism of shed vortex formation and its dependence on the other elements of the secondary flow structure have not yet been well recognised.

The structure presented in Figure 1 points out the existence of a dividing stream surface whose trace is recognised as a separation line between the secondary flow and the main stream at the blade suction side. In viscous flow it means the existence of a shear layer which may produce a significant loss.

The passage vortex and a pressure side branch of the horse shoe vortex have a clockwise sense of rotation in our illustration. In contrary the trailing shed vortex and a suction side horse shoe vortex have an anticlockwise sense of rotation. There is still an open discussion whether the pressure side branch of the horse shoe vortex is interlocked with the passage vortex or preserves its individuality. The result of this interaction may be strongly dependent on the cascade parameters. It is also not clear whether the suction side branch of the horse shoe vortex dissipates within the passage and how it interacts with the trailing shed vortex.

3. **Objective and scope of the investigation**

Experimental analysis of the 3-D structure of the secondary flow is very difficult and limited to the particular technical abilities of the wind tunnel. Access to the blade passage is always hard. Due to these reasons experimental results are limited to some areas which were made accessible for the measurement systems. The limitations of the measurement possibilities affect the data reduction process and also limit the extent of conclusions which follow from the measurements [6].

Numerical analysis allows for the most throughout analysis of the flow because it delivers full field data. There has always been the question of the CFD ability to reproduce all details of the complex, 3-D viscous and turbulent secondary flows. Numerical simulations of such complex flows put high demands on the code quality and resolution in order to be successful in this respect. The SPARC code [1] used in our group and recently assembled cluster of PC's provide all the necessary conditions to reach the goal.

In this paper we would like to present the ability of our CFD analysis in the detailed study of the secondary flows. This constitutes a platform on which research concerning secondary flow control and coolant injection effects will be carried out.

In order to have a good verification basis for our results the data from the Workshop [2] on Turbomachinery Cascades were used. This provides results of experimental investigations as well as corresponding numerical results of some research groups.

On the basis of the numerical simulations the analysis of the structure of secondary flows will be carried out in order to see if the obtained results are useful for detection and understanding of the streamwise vortices formed in the cascade flow field.

4. **Numerical approach**

The SPARC solver developed in Karlsruhe [1] was used. It solves the Navier-Stokes equations for viscous, compressible and turbulent flow.

Averaged equations of conservation (Favre averaging) for viscous, compressible flow, with a moving grid at local velocity $\vec{V}_{grid}$ in Cartesian, stationary reference co-ordinate system reads:

$$\iiint_V \frac{\partial \vec{U}}{\partial t}\,\mathrm{d}V + \iint_S \vec{F}\circ\vec{n}\,\mathrm{d}S + \iint_S \vec{G}\circ\vec{n}\,\mathrm{d}S = 0$$

where:

$\vec{U} = \begin{bmatrix} \rho(\vec{x},t) \\ \rho u_i(\vec{x},t) \\ \rho E(\vec{x},t) \end{bmatrix}$ – is the solution vector,

$\vec{F} = \begin{bmatrix} \rho(u_j - u_{gj}) \\ \rho u_i(u_j - u_{gj}) + p\delta_{ij} \\ \rho E(u_j - u_{gj}) + p u_j \end{bmatrix}$, $\vec{G} = \begin{bmatrix} 0 \\ \sigma_{ij} \\ u_k\sigma_{jk} + k\dfrac{\partial T}{\partial x^j} \end{bmatrix}$ – convective and viscous fluxes,

$\sigma_{ij} = \mu\left(\dfrac{\partial u_i}{\partial x^j} + \dfrac{\partial u_j}{\partial x^i}\right) - \dfrac{2}{3}\mu\delta_{ij}\dfrac{\partial u_k}{\partial x^k}$ – stress tensor.

The above set of equations, supplemented by the state equation of ideal gas, Sutherland's law for viscosity and turbulence model is discretised basing on control volume method for colocated arrangement, where all flow variables are linked to the volume centre.

For one cell, the spatial discretisation can be formulated as:

$$\frac{\mathrm{d}}{\mathrm{d}t}\left[\vec{w}_{ijk}(t)V_{ijk}(t)\right] + F_w^R\left[\vec{s}^{\,l}(t);\vec{w}(t)\right] = 0$$

where:

$\vec{w}_{ijk} = [\rho(t), \rho u_i(t), \rho E(t)]_{ijk}^T$ – solution vector,

F_w^R – residuum function, is evaluated by summing the fluxes through the cell faces,

$\vec{s}^{\,l}$ – external versor normal to the control volume face.

Grid movement affects only the convective fluxes. The central difference scheme with the numerical diffusion of Jameson type is used for the interpolation of convective and diffusive fluxes at the cell faces. In the case of present calculations the grid velocity is set to zero.

SPARC code is equipped with several numerical schemes and with a number of turbulence models.

5. Flow configuration

The basic configuration for the numerical simulation is the Duhram Low Speed Turbine Cascade [2], whose details were taken from the workshop report. The profile shape and the relative location of the measurement traverses are presented in Figure 2.

The cascade flow parameters are given in Table 1.

This cascade flow case concerns rather small Mach number. The maximum velocity in the blade passage reaches about $M = 0.2$. For the compressible solver it is low but still sufficient. In order to increase the quality of the calculation the double precision has been used. The behaviour of the solution convergence did not indicate any problems corresponding to the low values of flow velocity.

Introductory calculations in 2-D space allowed for optimisation of flow space discretisation. The division to blocks in 3-D is presented in Figure 3. This domain decomposition is necessary to allow for parallel computing and for grid optimisation. Computations have

Table 1. Cascade and flow parameters

inlet angle	42.75°
outlet angle	−68.6°
profile chord length	224 mm
axial chord	181 mm
cascade pitch	191 mm
blade half-span	200 mm
Reynolds number	4×10^5
inlet dynamic pressure	215 Pa
inlet velocity	19.1 m/s
inlet density	1.179 kg/m^3
dynamic viscosity	1.814×10^{-5} Ns/m^2

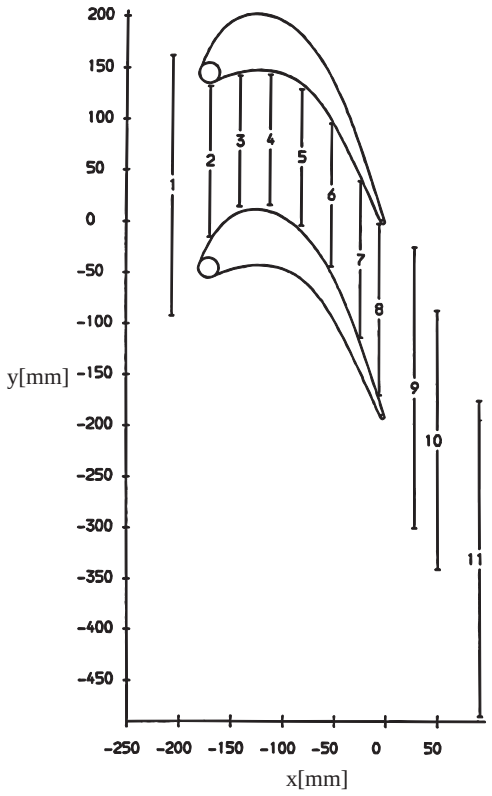

Figure 2. Duhram Low Speed Turbine Cascade [2]

been carried out on the PC cluster of IMP PAN for which 12 processors have been used. 3-D test calculations have shown that 1.8 million control volumes were necessary in order to obtain satisfactory results.

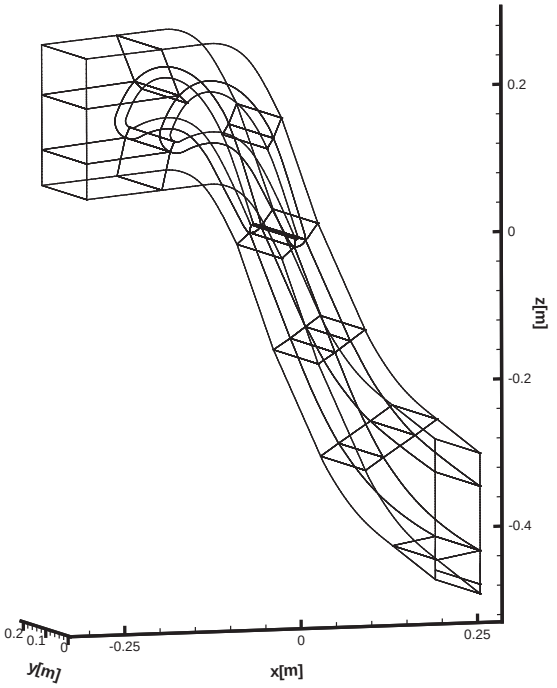

Figure 3. Domain decomposition

6. **Spanwise distribution of flow parameters**

The characteristic effect of secondary flows is displayed already by the spanwise distribution of the flow parameters as stagnation pressure loss and the flow angle downstream the cascade. Pitchwise averaged parameters are determined for each pitchwise plane (parallel to the side wall) and provide averaged values. The averaging is done taking into account equations of mass, momentum and energy, following the work of Amecke [7].

In Figure 4 spanwise distributions of stagnation pressure and yaw angle are presented.

It shows a comparison between obtained numerical results and experiment. $Y = 0$ denotes the side wall location. In the mid-span of the blade passage both quantities display an excellent coincidence with the experiment. Closer to the side wall calculated averaged yaw angle distribution is also in good agreement with experiment. This good coincidence shows that the numerical simulation describes very well the velocity field. It is a very important finding because the present aim is to study the development of streamwise vortices.

The pressure losses in the secondary flow area (close to the side wall) are predicted to be much lower than indicated by the experiment. Regarding the good prediction of the profile loss in the passage at mid-span it has to be concluded that the prediction of loss generation in the secondary flow area fails, underestimating it in this complex flow domain.

It should be mentioned however, that in comparison with results of other numerical simulations presented at the workshop [2] our results are very good. The agreement of our simulations with experiment is much better than any other.

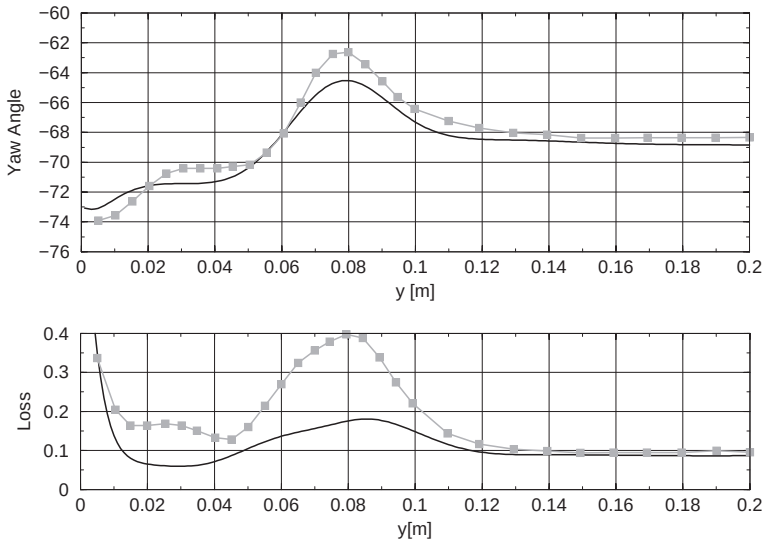

Figure 4. Spanwise distribution of homogeneous parameters: gray line – experiment, black line – numerical results

7. **Flow structure at the outlet from the cascade**

Results provided in [2] allow for useful comparison at one traverse plane (named 10 in Figure 2) downstream the cascade. Comparison of secondary velocity vectors is presented in Figure 5. These vectors are the result of subtraction of the local velocity vector from the velocity vector at the passage centre. The resulting vector is then projected on the traverse plane. The plane is parallel to the cascade trailing edge front and is located downstream in the distance 28% of axial chord length. The value of $Y = 0$ denotes location of the side wall, whereas $Y = 0.2$ the passage middle plane.

The comparison shows a very good coincidence of our results with experiment. The existence of two contra-rotating vortices is evident with a narrow zone in between, forming sort of a jet. This good coincidence confirms the observed agreement of values of flow angle in spanwise distribution in Figure 1.

Further comparison is presented in Figure 6.

It concerns stagnation pressure losses defined as:

$$Cp_{tot} = \frac{P_{tot1} - P_{tot}}{\frac{1}{2}\rho_2 v_2^2}$$

This expression provides a stagnation pressure coefficient defined as stagnation pressure difference between the local value and the inlet normalised by the dynamic head at outlet. In both plots the value scale of contours is identical.

In presented plots the wakes are visualised very well, as well as loss concentration due to the secondary vortices formation. The location and number of loss maxima coincide very well with experiment. The quality of this coincidence is much better than in all numerical results presented in [2]. This indicates that the flow structure is very well modelled by our simulations.

The main discrepancy is that losses value in the obtained maxima reach only half of the experimental value. It should be however realised that these maxima of losses are

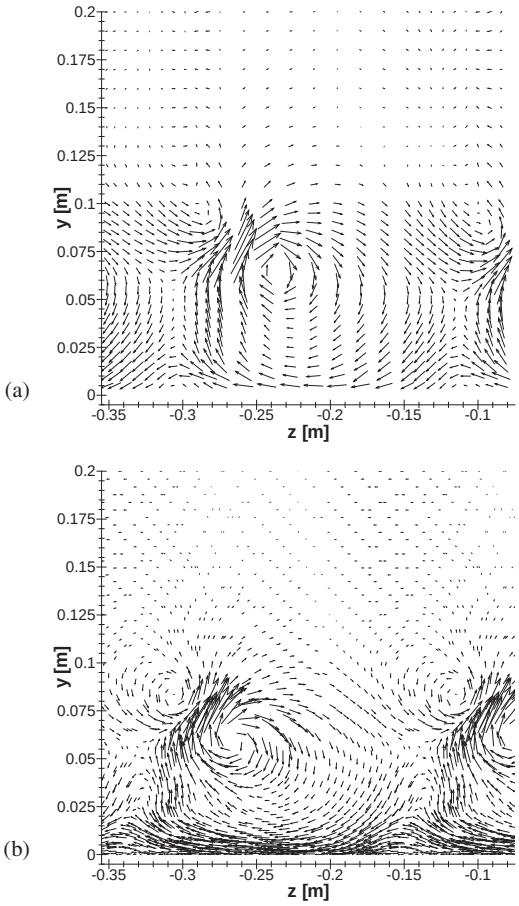

Figure 5. Secondary velocity vectors at outlet plane: (a) experiment; (b) numerical simulation

formed by the convection of mass from the incoming boundary layer into the centres of streamwise vortices and also due to the significant shear in the highly 3-D secondary flows. Very good prediction of profile losses in the passage middle shows that the losses due to the boundary layer are modelled well. Therefore one may conclude that the underestimation of loss value at maxima is due to insufficient modelling of losses at free, 3-D shear layers.

In order to have a better illustration of the flow structure in Figure 7 the losses contours were combined with the secondary flow vortices.

From this presentation it becomes apparent that the losses maxima concentrate in the centres of streamwise vortices.

Another method of the streamwise vortices visualisation is the distribution of vorticity. It is known that the vorticity value in the direction of vortex core displays the extremal values in the vortex. The sign of this extremum denotes the sense of rotation. This is a very useful feature which is used in Figure 8. It presents the distribution of vorticity component in the direction of the main stream, in order to visualise streamwise vortices. In Figure 8 secondary velocity vectors are also plotted.

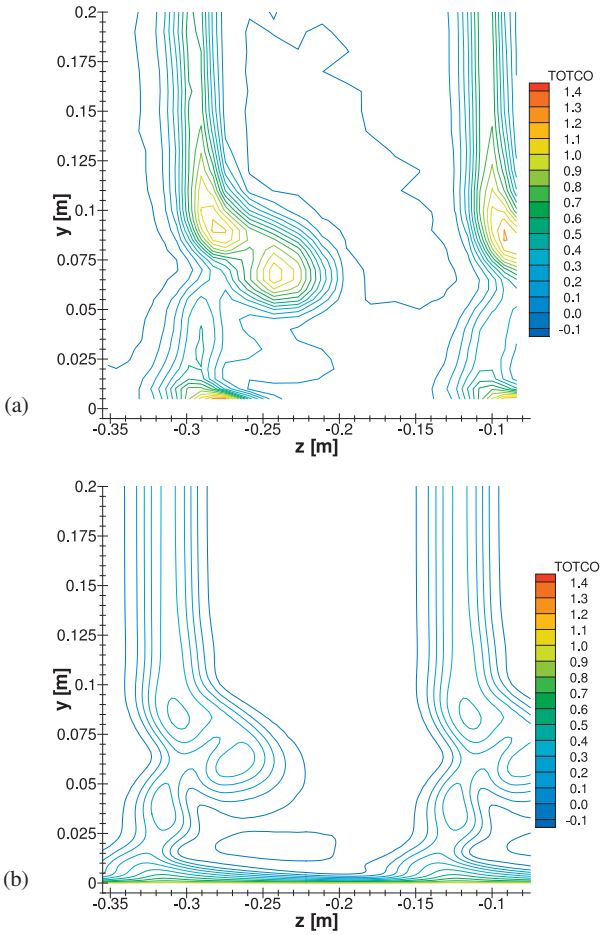

Figure 6. Stagnation pressure losses: (a) experiment; (b) numerical simulation

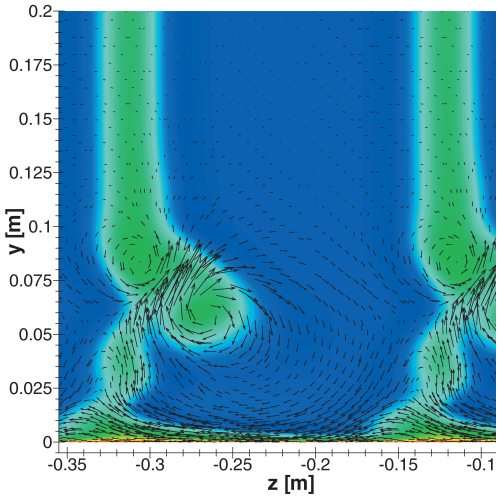

Figure 7. Losses contours and secondary velocity vectors

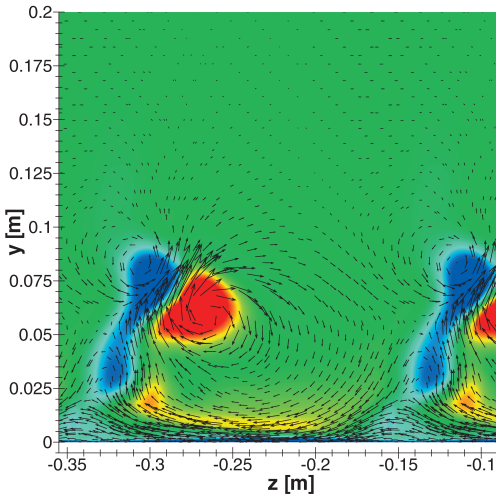

Figure 8. Streamwise vorticity contours and secondary velocity vectors

Figure 8 proves that the observed area of rotation with increased losses level represent streamwise vortices, one rotating in the different direction than the other. The analysis of vorticity field is important because its extremum confirms that the circular movement corresponds to a vortex. Generally, it is possible to find a helical movement of fluid which is not a vortex. Therefore, if the secondary flow is described as a system of secondary vortices one has to prove its existence by the vorticity field analysis.

8. Detection of streamwise vortices

The carried out simulations provided flow details in the whole calculation domain. In comparison with experimental research it is a new quality providing the possibility of access to every corner of the considered flow area. Good coincidence of the obtained results with available experimental data gives confidence to further analysis of the flow field. It should be realised, however, that the secondary flow structure and the results of interaction between streamwise vortices are strongly dependent on the general features of the cascade parameters. Streamline curvature in the blade passage and ratio of leading edge radius to side wall boundary layer thickness being the main factors here.

One of the main items of secondary flow is the horse shoe vortex (Figure 1). It is formed by the leading edge submerged in the side wall boundary layer. At the leading edge it is divided to the suction side branch and the pressure side branch. This vortex has been visualised by the tracer streaks in Figure 9. Black lines concern suction side branch of the horse shoe vortex and red lines a pressure side one.

One important observation may be drawn from Figure 9. The suction side branch of the horse shoe vortex winds up around the pressure side one at the cascade outlet. The pressure side vortex is usually incorporated into the passage vortex. In consequence it indicates that also the suction side vortex is incorporated by the passage vortex.

In order to look closer into this problem in Figure 10 the streaks originating inside the side wall boundary layer within the blade passage have been included.

In Figure 10 some blue lines wind up around both branches of the horse shoe vortex. This confirms that in the case of the considered cascade the suction side of the horse shoe

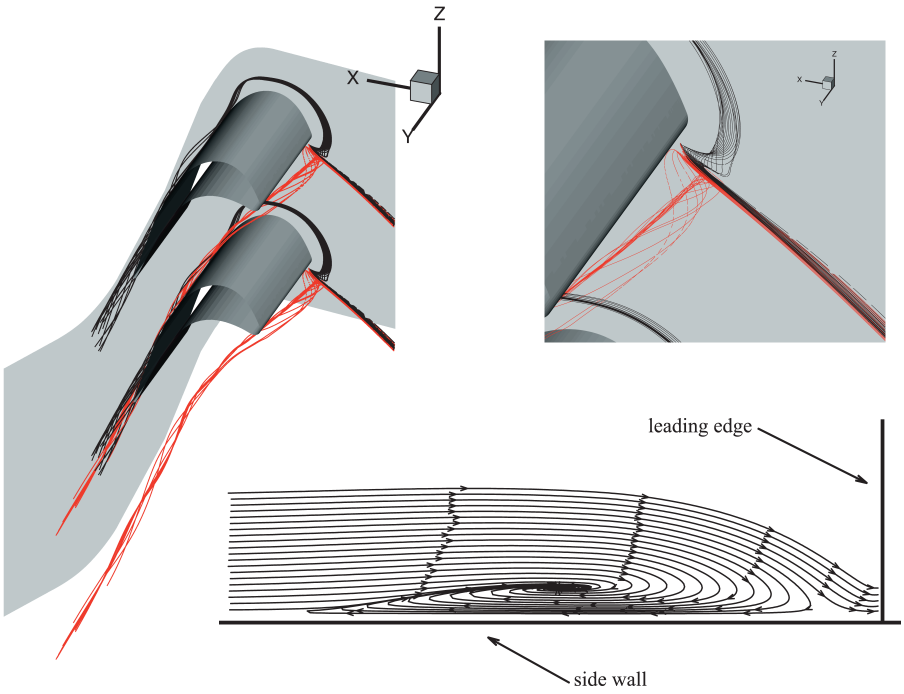

Figure 9. Horse shoe vortex: red – pressure side, black – suction side

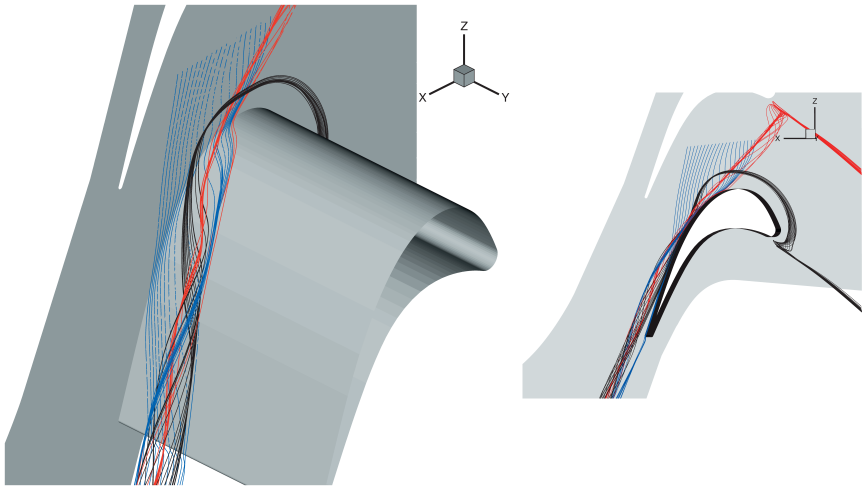

Figure 10. Horse shoe vortex with passage vortex: red – pressure side, black – suction side, blue – passage vortex

vortex integrates with the passage vortex in spite of the fact that it has originally an opposite sense of rotation.

Another part of the streaks originating at the side wall flows along the blade suction side down to the trailing edge without being lifted into the passage vortex. It is well visible at the small projection picture in Figure 10.

Additional observation concerning passage and horse shoe vortex configuration may be drawn from Figure 11 where the sectional plane with the streamwise vorticity map (from Figure 8) is included. It now becomes evident that both branches of the horse shoe vortex (black and red) are passing though the same vortex, namely the passage vortex. Blue lines are passing through the passage vortex and partly through the vortex of the other sense of rotation. This second part is the one that flows over the trailing edge.

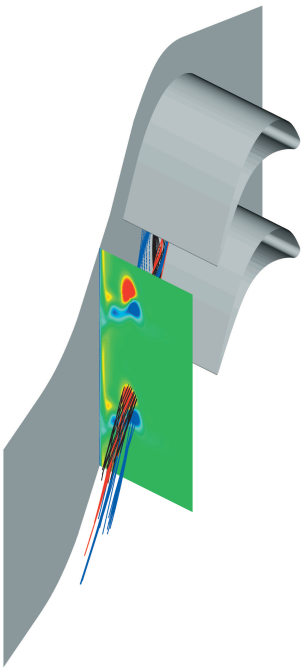

Figure 11. Streamwise vortices tracers with vorticity plane

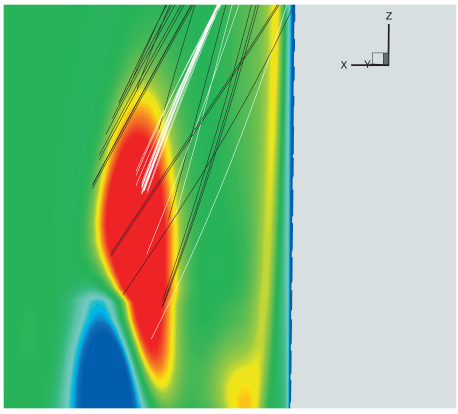

Figure 12. Horse shoe vortices inside the passage vortex

A closer look is presented in Figure 12 which is a close up of Figure 11. It is a view from the trailing edge on the vorticity plane and shows the penetration of the horse shoe

vortex through the passage vortex. For better contrast the streaks belonging to the pressure side branch of the horse shoe vortex are given a white colour instead of red.

Two important conclusions may be drawn from this picture:

- pressure side branch is incorporated into the centre of the passage vortex, which is in accordance with general understanding,
- the streaks of the suction side vortex are distributed around the passage vortex, which is a new observation and means that this branch of the horse shoe vortex is destroyed by the passage vortex and that the suction side of the horse shoe vortex does not exist at this location.

Another important element of the secondary flow structure is the trailing shed vortex. As it was mentioned before it is expected to be formed by the folding of the vorticity sheet originating behind the trailing edge. Its sense of rotation is opposite to the passage vortex and is the same as the suction branch of the horse shoe vortex at its origin.

In Figure 13 a plan view onto the trailing edge is presented, the side wall is to the left. Streaks are originating within boundary layer shortly upstream of the trailing edge. The suction side streaks are black and the pressure side streaks are red. Downstream the trailing edge the concentration of streaks takes place. Between this location and the side wall there is a strong cross flow inducing vorticity sheet. It should be noticed that the concentration of streaks starts already upstream the trailing edge. Therefore it is doubtful that the mechanism of the trailing shead vortex formation is folding of the vorticity sheet itself. This folding is induced by the streamwise vortices, formed within the blade passage.

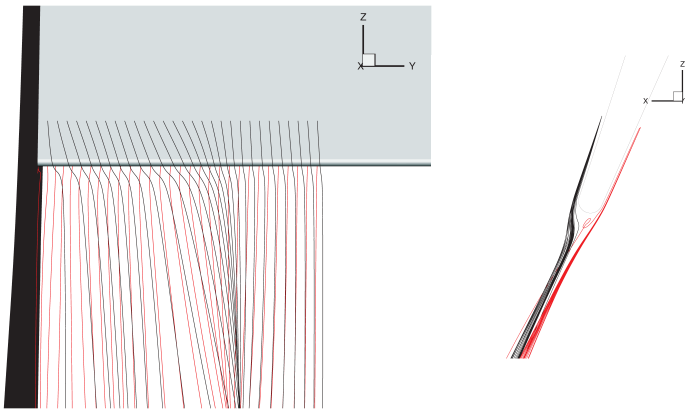

Figure 13. Trailing shed vortex formation

For the better insight into the details in Figure 14 the trailing edge streaks are presented together with vorticity plane in the view as in Figure 12. It becomes evident here that the main contribution to the streamwise vortex rotating opposite to the passage vortex is the wake contaminated with the railing shead vorticity. It also shows that the shed vorticity is present only in the side wall neighbourhood as far as the extent of the secondary flow. Looking at the close up in Figure 14 it may be noticed that the expected winding up of the pairs of red and black lines is very weak. Therefore, the main reason for the local vorticity extremum (blue) is the flow field deformation by the passage vortex.

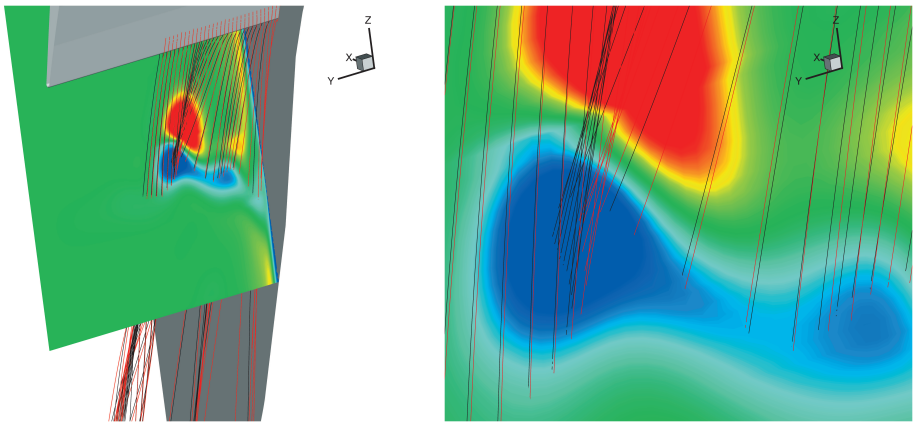

Figure 14. Trailing edge streaks passing through the vorticity plane

9. Conclusions

The carried out numerical analysis of the secondary flow has proven that the SPARC code and the used PC's cluster provide a powerful and very efficient tool for the analysis of such a complicated flow field. Good coincidence of calculation results with experiment proves that the presented attempt is very successful and gives confidence in further analysis of the physical processes involved.

Bearing in mind that the secondary flow structure and the results of interaction between streamwise vortices are strongly dependent on the general features of the cascade parameters one may conclude that in the considered cascade flow case:

- pressure side branch of the horse shoe vortex is incorporated into the passage vortex and apparently is located in its centre,
- suction side horse shoe vortex is dissipated by the passage vortex,
- the vorticity opposite to the passage vortex is generated in the wake and has nothing to do with the suction side horse shoe vortex,
- the formation of trailing shed vortex is due to the action of the passage vortex.

The above conclusions could be drawn only thanks to the numerical simulations. Experimental investigation is not able to provide answers concerning the history of streamwise vortices because the access to the flow field is limited. Only numerical investigation provides field data which are essential in order to analyse all aspects of the flow field development.

References

[1] Magagnato F 1998 *TASK Quarterly* **2** 215
[2] Gregory-Smith D G 1994 *Turbomachinery Workshop Test Case* **3** 116
[3] Sieverding C H 1985 *ASME, Journal of Eng. for Gas Turbines and Power* **107** 248
[4] Gregory-Smith D G, Greves C P and Walsh J A 1988 *ASME, Journal of Turbomachinery* **110** 1
[5] Basis F, Osnaghi C, Perdichizzi A and Savini M 1989 *ASME, Journal of Fluids Eng.* **111** 369
[6] Doerffer P P and Amecke J 1994 *IGT&AC Congress, ASME paper 94-GT-376* The Hague, Netherlands – June 13–16
[7] Amecke J 1970 *Anwendung der transsonishe Aehnlichkeitsregel auf die Stroemung durch ebene Schaufelgitter*, VDI-Forschungsheft